

Self-Assembled Monolayers of ω -Biphenylalkanethiols on Au(111): Influence of Spacer Chain on Molecular Packing

Piotr Cyganik,[†] Manfred Buck,^{*,†} Waleed Azzam,[‡] and Christof Wöll^{*,‡}

School of Chemistry, University of St. Andrews, North Haugh, St. Andrews, Fife KY16 9ST, United Kingdom, and Lehrstuhl für Physikalische Chemie I, Universitätsstrasse 150, 44801 Bochum, Germany

Received: October 31, 2003; In Final Form: January 28, 2004

Self-assembled monolayers (SAM) of ω -(4'-methylbiphenyl-4-yl)alkanethiols $\text{CH}_3(\text{C}_6\text{H}_4)_2(\text{CH}_2)_n\text{SH}$ (BP n , $n = 1-6$) on Au(111) substrates, prepared at room and elevated temperatures, were studied using scanning tunneling microscopy (STM). Molecularly resolved images reveal that all BP n SAMs form well-ordered layers over areas easily exceeding $50 \times 50 \text{ nm}^2$. Only two basic structures are alternately adopted with n changing between odd and even. The unit cell of odd-numbered SAMs is described by an oblique $(2\sqrt{3} \times \sqrt{3})R30^\circ$ structure and contains two molecules. In contrast, the even-numbered SAMs are described by a much larger, rectangular $(5\sqrt{3} \times 3)$ structure with eight molecules per unit cell and occupying an area per molecule larger by about 25% compared to $n = \text{odd}$. With the exception of BP1 and BP6 the preparation at elevated temperatures resulted in a significant improvement in structural quality, yielding very large domains. For BP6 prepared at 343 K a strong domain anisotropy is observed, which is explained by the influence of the alkane spacer chain. For BP1 prepared at 343 K formation of gold islands is concluded.

I. Introduction

Studies of fundamental aspects of film formation, structure, and properties of self-assembled monolayers (SAM) of thiols have been overwhelmingly based on alkanethiols.¹⁻⁷ Only recently, aromatic thiols have also moved into the focus of interest⁸⁻²⁷ since they represent an interesting alternative to alkane-based thiol SAMs. Because of their higher rigidity and stronger intermolecular interactions compared to those of their aliphatic counterparts, aromatic thiols offer the chance of better control over the structure of SAMs. Furthermore, they contrast alkanethiols with respect to a number of properties such as the behavior toward electron irradiation²⁸ or charge-transfer properties,²⁹⁻³¹ which makes them interesting for molecular electronics³²⁻³⁴ and electrode modification.^{35,36} Many of these applications require a precise control of SAMs down to the length scale of molecular dimensions since a number of SAM properties are critically dependent on details of the SAM structure. This is highlighted by theoretical calculations³⁷⁻⁴² and experiments,⁴³⁻⁴⁶ where the electronic properties were found to strongly depend on molecular orientation, contact geometry and bonding, and intermolecular interactions. The molecular packing and the influence of defects and domain boundaries on the overall properties of SAMs are therefore crucial issues which require a detailed knowledge of the relevant factors and interactions involved such as intermolecular forces, substrate properties, and molecule-substrate interactions.

Along our efforts toward a rational design of organothiol SAMs and an understanding of the relationship between the structures of thiol SAMs and the structure of the respective molecules, we have focused on a homologue series of molecules which are characterized by a biphenyl moiety attached to the thiol group via an alkane spacer of varying length ($\text{CH}_3-(\text{C}_6\text{H}_4)_2-(\text{CH}_2)_n-\text{SH}$, BP n , $n = 1-6$). Previous spectroscopic studies^{19,47} revealed a strong influence of the S-Au interface

on the film structure. The films were found to exhibit a pronounced alternation in molecular orientation and coverage with length of the alkane chain changing between $n = \text{odd}$ and $n = \text{even}$ (Figure 1), which is reflected in a number of properties such as stability toward exchange³¹ and in electrochemical environment⁴⁸ or electron-induced modification of film structures.⁴⁹ The spectroscopic observations were explained by a simple model considering intermolecular interactions and the C-S-Au bending potential¹⁹ (see below). A recent scanning tunneling microscopy (STM) study for BP3 and BP4 on Au(111) revealed pronounced odd-even differences in the molecular packing,⁵⁰ in full agreement with the spectroscopic observations.

The present STM investigation extends the preceding work on these systems^{19,47,50,51} by analyzing structural details within the homologue BP n series with n ranging from 1 to 6. Studying the series of BP n SAMs should reveal whether the odd-even effect is an alternation between exactly two different structures or whether the change in length of the alkane spacer which introduces additional interactions and degrees of freedom affects substantially the free energy of the SAMs and, thus, yields additional structural features. A closely related issue of interest in this study is also how the preparation temperature affects the structural quality of the BP n films and their spacer-dependent structures.

II. Experimental Section

Sample Preparation. The synthesis of the biphenyl series BP n ($n = 1-6$) has been described elsewhere.¹⁹ Au substrates were prepared by thermal evaporation of 150–200 nm thick layer of gold (99.99%, Chempur) on mica substrate at 320 °C in the vacuum chamber with the base pressure of 2×10^{-7} Torr. Before evaporation mica was heated by 24 h at the same temperature. The evaporation rate (20 Å s^{-1}) was monitored using a crystal oscillator (Leybold Inficon). After deposition the substrates were cooled, and the vacuum chamber was vented with nitrogen. The substrates were stored under nitrogen and flame-annealed in a butane/oxygen flame immediately before the adsorption experiments were carried out. This procedure

[†] University of St. Andrews.

[‡] Lehrstuhl für Physikalische Chemie I.

* Corresponding authors: e-mail mb45@st-and.ac.uk (M.B.); e-mail woell@pc.ruhr-uni-bochum.de (C.W.).

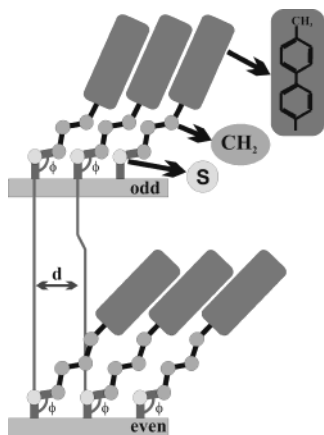


Figure 1. Illustration of BP n SAMs on gold with odd (a) and even numbers (b) of methylene groups. For n = even the intermolecular distance d is larger and the aromatic units are more tilted than for n = odd due to the influence of the C–S–Au bending potential, i.e., angle ϕ .

yielded Au(111) substrates with terrace widths typically in the range 100–500 nm.

The BP n monolayers (n = 1–6) substrates were prepared on Au(111) either at room temperature, at 333 K, or at 343 K by immersing the gold substrates into dilute ethanolic solutions (100 μ M) of the respective thiol. After 24 h of incubation, substrates were removed from the solution, rinsed with pure ethanol, and dried in a nitrogen stream.

STM Measurement. All STM measurements were carried out in air using two different STM instruments: a PicoSPM (Molecular Imaging) and a Nanoscope III (Digital Instruments). In all cases tips were prepared mechanically by cutting a 0.25 mm Pt/Ir alloy (8:2, Chempur) wire. The data have been collected in constant-current mode using tunneling currents between 200 and 700 pA and a sample bias between 200 mV and 1.3 V (tip positive). The interpretation of our data is based on the assumption that the tip does not disturb the layer. This appears to be well justified since, first, under all conditions no tip-induced changes were seen even after repeatedly scanning the same area on the sample. Second, it has been demonstrated that under similar imaging conditions it is possible to image the structural details of the (4×2) superstructure of alkanethiolate SAMs (tunneling current and voltage of 280 pA and 0.54 V, respectively).⁵² Since the conductivity of the biphenylthiolate backbone is significantly higher^{13,14} because of the smaller HOMO–LUMO gap, it is very likely that the surface of the BP n SAM, i.e., the methyl termini, is mapped rather than the tip penetrates the layer. This is further supported by the fact that the modulation of the tunneling current by the SAM is strongly dependent neither on the length of the alkane spacer (e.g., BP3 compared to BP5) nor on the tunneling conditions.

III. Results

Figures 2–7 show STM data of BP n SAMs with odd (Figures 2–4) and even (Figures 5–7) numbers of methylene spacer units. In each figure the low- and high-resolution STM images labeled (a) and (c) represent samples prepared at room temperature (RT). Images with corresponding resolution for samples prepared at elevated temperatures of 333 or 343 K are shown in (b) and (d). Comparison of (a) with (b) and (c) with (d), thus, allows to judge the influence of preparation temperature on film morphology at different length scales. Images labeled (e) show STM data recorded at high (molecular) resolution.

For a given BP n SAM the STM images recorded at room temperature, and elevated temperature did not reveal any dif-

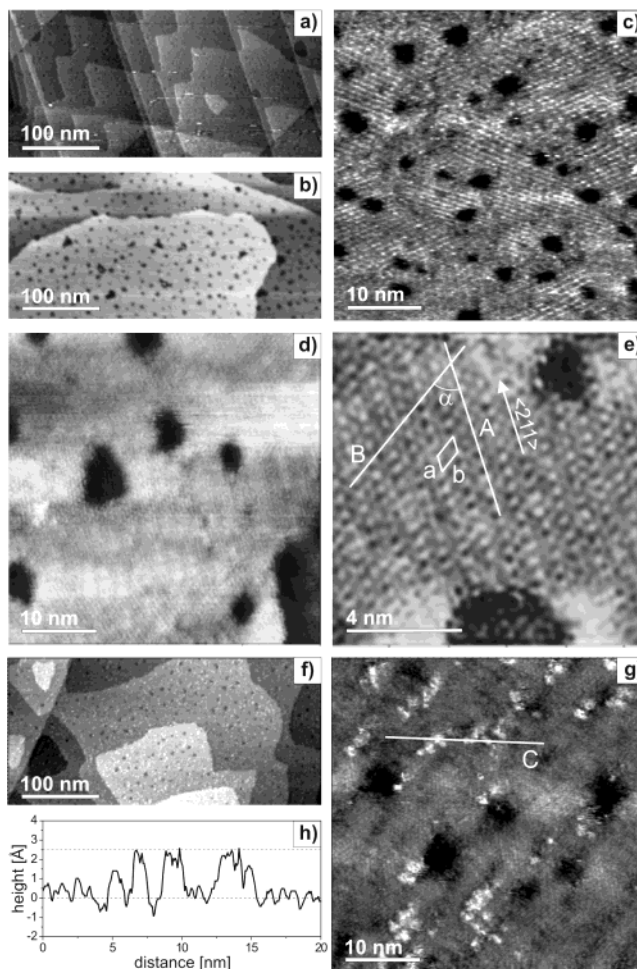


Figure 2. SAM of BP1 on Au(111). STM images at different resolution show samples prepared at room temperature (a, c), at 333 K (b, d, e), and at 343 K (f, g). Oblique box depicted in (e) marks the ($\sqrt{2} \times 3\sqrt{3}$)/ $R30^\circ$ oblique unit cell. Its average size ($a = 5.1 \pm 0.5$ Å, $b = 10.2 \pm 0.8$ Å, and $\alpha = 57 \pm 3^\circ$) was calculated from the cross-sectional height profiles taken along the directions marked by lines A and B for a set of five different images. (h) represents the height profile along line C shown in (g). Tunneling parameters: (a) $U = 1.2$ V, $I = 520$ pA; (b) $U = 0.5$ V, $I = 210$ pA; (c) $U = 1.2$ V, $I = 500$ pA; (d, e) $U = 0.5$ V, $I = 210$ pA; (f, g) $U = 0.8$ V, $I = 200$ pA.

ferences in the shape or the size of the unit cell. Since the overall quality and the ease at which molecular resolution is achieved are higher compared to room temperature, the high-resolution data shown in (e) have all been recorded for annealed samples.

Features Common to All BP n SAMs. One of the features shared by all BP n SAMs is the depressions appearing as dark islands in the STM images. As described previously,^{53–56} these “pits” represent vacancy islands in the topmost layer of gold atoms formed during the self-assembly process. Also, the dependence of island size on preparation temperature is similar for all different SAMs studied here. Comparison of SAMs prepared at room temperature with SAMs formed at elevated temperature reveals a pronounced increase in size and a corresponding decrease in density of the vacancy islands due to Ostwald ripening.^{57,58} Also, the average domain size increases substantially with increasing temperature.⁵⁹ At room temperature domains exhibit sizes in the range 5–20 nm for all BP n SAMs. Domain sizes at elevated temperatures depend on the spacer length and can reach 70–100 nm for shorter spacers ($n < 4$) whereas the upper values for $n = 4, 5$ range between 40 and 60 nm. As discussed in more detail later, $n = 6$ represents a

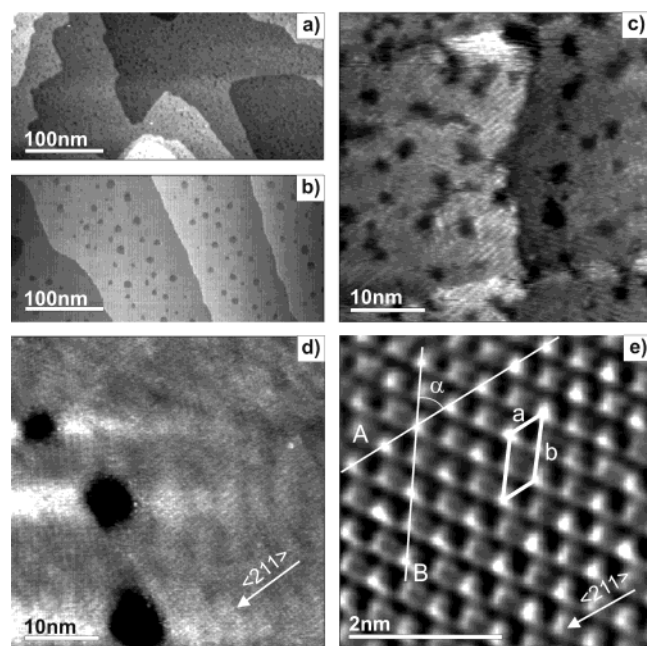


Figure 3. SAM of BP3 on Au(111). STM images at different resolution show samples prepared at room temperature (a, c) and at 343 K (b, d, e). Oblique box depicted in (e) marks the $(\sqrt{2} \times 3\sqrt{3})R30^\circ$ unit cell. Its average size ($a = 5.2 \pm 0.5 \text{ \AA}$, $b = 9.5 \pm 0.7 \text{ \AA}$, and $\alpha = 59 \pm 3^\circ$) was calculated from the cross-sectional height profiles taken along the directions marked by lines A and B for a set of five different images. Tunneling parameters: (a–f) $U = 0.9 \text{ V}$, $I = 600 \text{ pA}$.

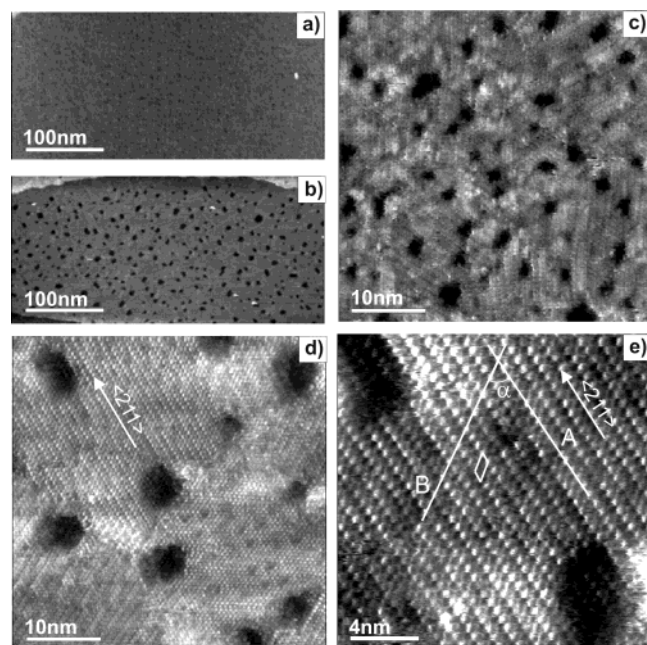


Figure 4. SAM of BP5 on Au(111). STM images at different resolution show samples prepared at room temperature (a, c) and at 343 K (b, d, e). Oblique box depicted in (e) marks the $(2\sqrt{3} \times \sqrt{3})R30^\circ$ unit cell. Its average size ($a = 5.2 \pm 0.4 \text{ \AA}$, $b = 9.6 \pm 0.8 \text{ \AA}$, and $\alpha = 60 \pm 3^\circ$) was calculated from the cross-sectional height profiles taken along the directions marked by lines A and B for a set of five different images. Tunneling parameters: (a) $U = 1 \text{ V}$, $I = 570 \text{ pA}$; (b) $U = 1 \text{ V}$, $I = 400 \text{ pA}$; (c) $U = 1 \text{ V}$, $I = 500 \text{ pA}$; (d, e) $U = 1.3 \text{ V}$, $I = 600 \text{ pA}$.

special case due to the anisotropic shape with 10–30 nm along $\langle 110 \rangle$ and 4–15 nm along $\langle 211 \rangle$.

Odd-Numbered BP n SAMs. As inferred from the height profiles along lines A and B indicated in Figures 2e–4e, all odd-numbered BP n SAMs form the same structure described

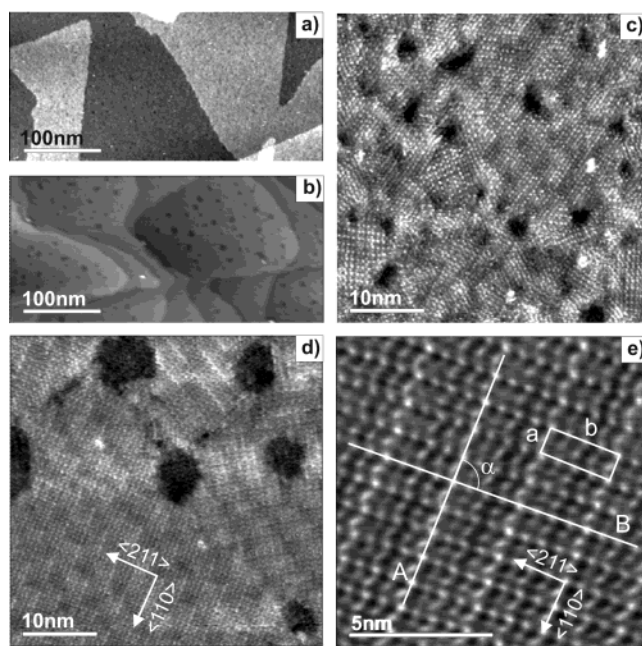


Figure 5. SAM of BP2 on Au(111). STM images at different resolution show samples prepared at room temperature (a, c) and at 343 K (b, d, e). Rectangular box depicted in (e) marks the $(5\sqrt{3} \times 3)\text{rect}$ unit cell. Its average size ($a = 8.9 \pm 0.8 \text{ \AA}$, $b = 24.3 \pm 1.1 \text{ \AA}$, and $\alpha = 90 \pm 3^\circ$) was calculated from the cross-sectional height profiles taken along the directions marked by lines A and B for a set of five different images. Tunneling parameters: (a–e) $U = 1 \text{ V}$, $I = 500 \text{ pA}$.

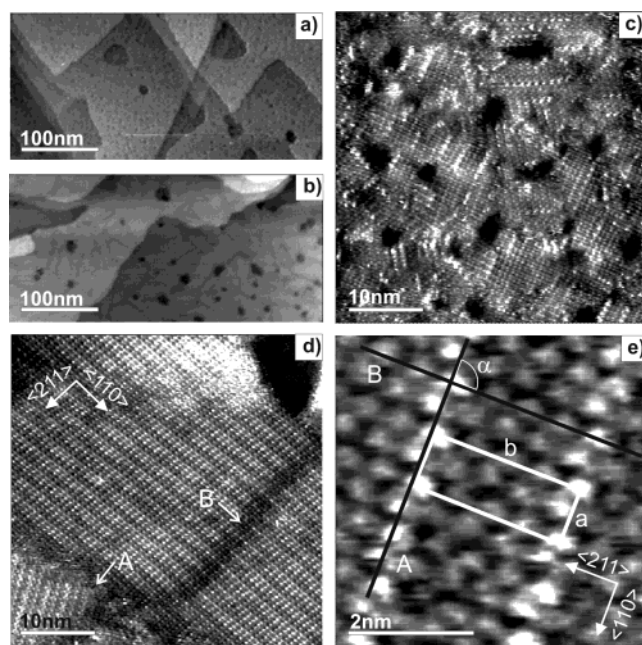


Figure 6. SAM of BP4 on Au(111). STM images at different resolution show samples prepared at room temperature (a, c) and at 343 K (b, d, e). Rectangular box depicted in (e) marks the $(5\sqrt{3} \times 3)\text{rect}$ unit cell. Its size ($a = 8.7 \pm 0.7 \text{ \AA}$, $b = 24.6 \pm 1.3 \text{ \AA}$, and $\alpha = 89 \pm 3^\circ$) was calculated from the cross-sectional height profiles taken along the directions marked by lines A and B for a set of five different images. Tunneling parameters: (a–d) $U = 1 \text{ V}$, $I = 600 \text{ pA}$; (e) $U = 0.7 \text{ V}$, $I = 600 \text{ pA}$.

by an oblique unit cell. Whereas the height modulation along the $\langle 211 \rangle$ direction exhibits a single periodicity around 5 \AA , there is an additional modulation of about 10 \AA along the $\langle 110 \rangle$ direction. This suggests that the commensurate $(2\sqrt{3} \times \sqrt{3})R30^\circ$ structure reported recently in an STM and LEED investigation of BP3⁵⁰ is a general feature of odd-numbered BP n

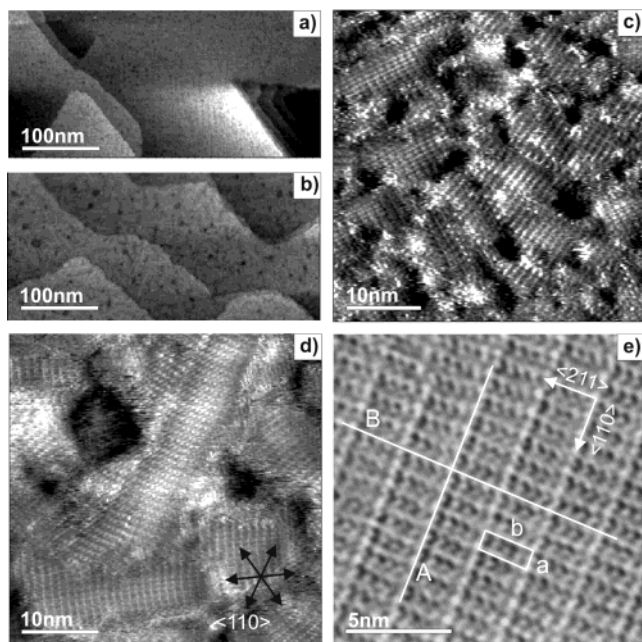


Figure 7. SAM of BP6 on Au(111). STM images at different resolution show samples prepared at room temperature (a, c), at 343 K (b, d) and at 333 K (e). Rectangular box depicted in (e) marks the $(5\sqrt{3} \times 3)$ rect unit cell. Its size ($a = 9.5 \pm 0.7$ Å, $b = 25.3 \pm 1.5$ Å, and $\alpha = 91 \pm 3^\circ$) was calculated from the cross-sectional height profiles taken along the directions marked by lines A and B for a set of five different images. To illustrate the alignment of the anisotropic domains the $\langle 110 \rangle$ directions indicated in (d). Tunneling parameters: (a–d) $U = 1$ V, $I = 600$ pA; (e) $U = 0.6$ V, $I = 160$ pA.

SAMs. However, as discussed in detail in a forthcoming publication,⁶⁰ for very large domain sizes a Moire-like structure is observed which indicates the presence of a weak incommensurability.

A simplified structural model of odd-numbered SAMs is presented in Figure 9a. Considering the van der Waals dimensions of the phenyl group (cross section in the plane perpendicular to the plane of the ring is 6.4 Å by 3.3 Å), a herringbone-like arrangement of the biphenyl backbones in the $(2\sqrt{3} \times \sqrt{3})R30^\circ$ unit cell is the simplest model consistent with the STM data.⁵⁰ As discussed in a preceding spectroscopic study, this model also fits well to the bulk structure of biphenyl.¹⁹ In this model, the phenyl planes are orientated roughly along the $\langle 211 \rangle$ -direction of the Au(111) lattice and form a herringbone-like arrangement with density of 21.6 Å² per molecule, i.e., the same packing density as in SAMs of alkanethiols. It is important to note that for clarity of presentation the structure presented in Figure 9a does not show the tilt of the molecules with respect to the substrate normal. This is, therefore, an oversimplified representation which does not explain the $(2\sqrt{3} \times \sqrt{3})R30^\circ$ unit cell since all molecules are identical. Additional factors, presently unknown, must lift the degeneracy, and possible reasons could be either slightly different adsorption sites or a tilt direction of the aromatic units off the glide plane.

However, despite a common unit cell structure, there are several slight differences in the packing of the odd-numbered BP n SAMs. In particular for BP1 it was found, for reasons which are not clear at present, that it is more difficult to achieve molecular resolution. Second, the preparation temperature is significantly more critical. Up to about 333 K (Figure 2b,d) BP1 behaves like BP3 and BP5; i.e., an increase in preparation temperature causes ripening of the edge pits and an increase in domain size. However, as demonstrated in Figure 2f–h, a new type of rather small protrusions (<2.5 nm in diameter) appear above this temperature. The line profile of Figure 2h exemplifies that most of the protrusions have a height of about 2.5 Å, suggesting a Au step. We will return to the issue of island formation, but already at this point we would like to note that

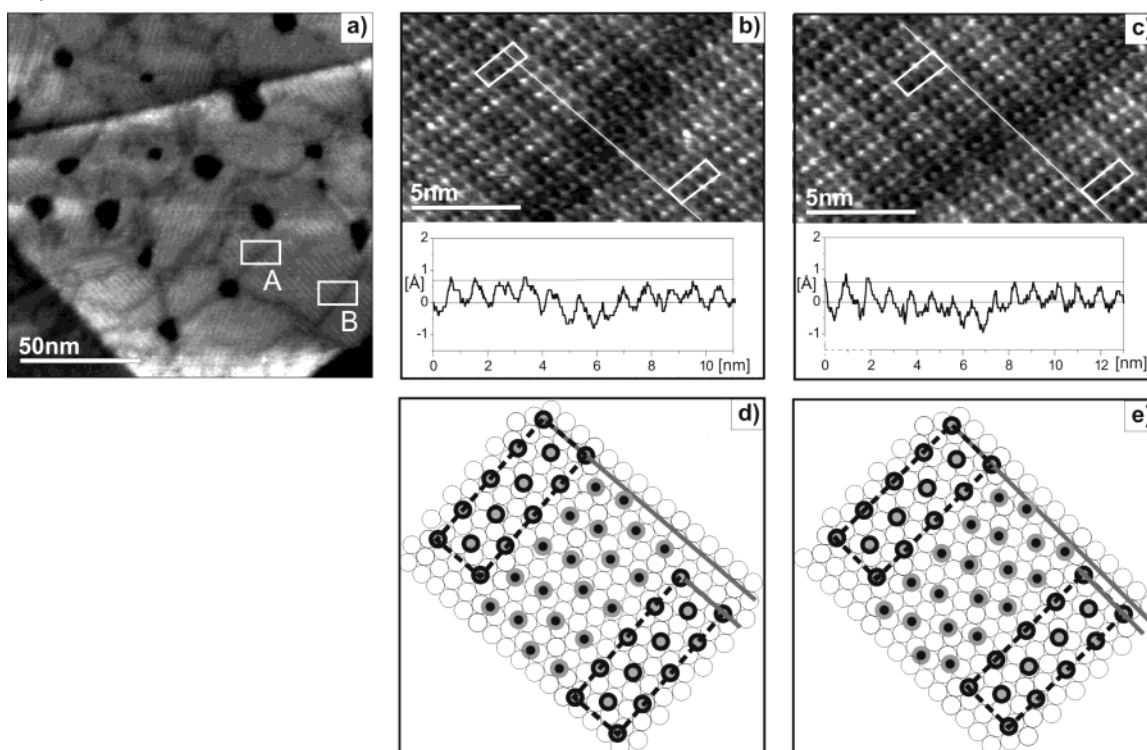


Figure 8. SAM of BP4 on Au(111) prepared at 343 K. (a) Larger scale STM image showing a network of dark lines which connect vacancy islands. Molecularly resolved images of areas A and B are depicted in (b) and (c), respectively. Boxes in (b) and (c) mark the $(5\sqrt{3} \times 3)$ rect unit cell and illustrate that the structure can remain unaltered (b) or experience a translational phase shift across a dark region. Height profiles taken in the images presented in (b) and (c) are shown in lower parts of (b) and (c), respectively. In (d) and (e) translational phase shift is illustrated for (b) and (c), respectively (see discussion in text). Tunneling parameters: (a, b, d) $U = 1$ V, $I = 600$ pA.

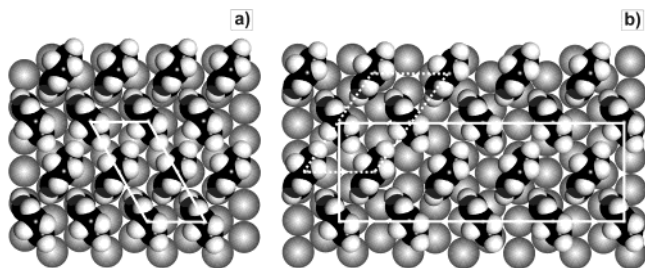


Figure 9. Illustration of molecular arrangements in SAMs of BP n on Au(111). (a) Top view of the $(2\sqrt{3} \times \sqrt{3})R30^\circ$ structure adopted by the odd-numbered SAMs and (b) top view of the $(5\sqrt{3} \times 3)\text{rect}$ structure of the even-numbered SAMs. Both in (a) and (b) the unit cells are assigned by white solid line. For the white dotted line in (b) see text (section IV). The molecules are drawn in upright orientation for clarity. In reality, they are inclined by about $23^\circ (\pm 7^\circ)$ for $n = \text{odd}$ and $45^\circ (\pm 10^\circ)$ for $n = \text{even}$.¹⁹ Note also the adsorption sites, e.g., the 3-fold hollow sites for BP3, have been chosen arbitrarily. The true position is not known.

the BP1 system could not be prepared with the same structure quality than the other SAMs studied here.

Even-Numbered BP n SAMs. Analogous to the odd-numbered series we observe a common unit cell for all even-numbered BP n SAMs. However, the structure for $n = \text{even}$ is strikingly different from those for $n = \text{odd}$, which is characterized by two molecules per unit cell and an oblique $(2\sqrt{3} \times \sqrt{3})R30^\circ$ structure. The STM data shown in Figures 5e–7e clearly show an orthogonal, commensurate structure with a periodicity defined by every second and fourth row of molecules along the $\langle 211 \rangle$ and $\langle 110 \rangle$ directions, respectively.⁵⁰ The size of the unit cell was determined from larger images (not shown) and fits well to a $(5\sqrt{3} \times 3)\text{rect}$ structure. The high-resolution image of BP4 (Figure 6e) shows the presence of eight molecules per unit cell, corresponding to an area per molecule of 27.05 \AA^2 . Compared to the 21.6 \AA^2 for odd-numbered BP n SAMs, this corresponds to a 25% lower packing density. As in the case of BP4,⁵⁰ also BP2 and BP6 exhibit different heights of the molecules within a unit cell. Even though the exact number of molecules appearing at different heights depends somewhat on the tunneling conditions, we observed as discussed in detail in a preceding publication⁵⁰ at least three different heights within a unit cell.

When comparing the structures of the odd- and even-numbered SAMs, we find that they share a structural feature, namely that every second row of molecules running along the $\langle 211 \rangle$ direction shows the same height in the STM images. For both odd and even systems, the distance between equivalent rows of molecules amounts to about 9 \AA . In addition, for $n = \text{even}$ every fourth row of molecules oriented parallel to the $\langle 110 \rangle$ direction exhibits the same height. The corresponding unit cell length amounts to 25 \AA along the $\langle 211 \rangle$ direction, corresponding to an intermolecular distance of 6.25 \AA , which is significantly larger than the value of 5 \AA observed for $n = \text{odd}$. Formally, the structure of the even-numbered BP n SAMs is, thus, obtained by anisotropic expansion of the $n = \text{odd}$ structure along the $\langle 211 \rangle$ direction.

Combining information from the STM images with the spectroscopic data¹⁹ which showed that on gold the biphenyl units in even systems are substantially more tilted than the odd systems, the structure shown in Figure 9b provides a model consistent with the experimental data. We suggest that for $n = \text{even}$ the molecules arrange in a herringbone-like fashion as for $n = \text{odd}$ but with the BP units more tilted along the $\langle 211 \rangle$ direction. However, in contrast to odd-numbered BP n SAMs where a bulklike packing of the biphenyl units is possible, the larger tilt angle of the BP units in the less densely packed, even-

numbered SAMs¹⁹ should reduce the interaction between the biphenyl units.

After the discussion of common features in even-numbered SAMs we focus now on differences within this series. While for all BP n SAMs preparation at elevated temperatures results in an overall increase in domain size, BP6 behaves very differently compared to the other two even-numbered SAMs. For $n = 2$ and 4 preparation at 343 K yields domain sizes easily exceeding $5 \times 10^3 \text{ nm}^2$ (see Figures 5d and 6d). The shape of the domains is rather isotropic and structurally ill-defined regions between domains with no molecular features resolved are, typically, only a few molecules wide. In contrast, as demonstrated by Figure 7d SAMs of BP6 prepared at elevated temperatures exhibit a pronounced anisotropy of the domains with the long axis oriented always along the $\langle 110 \rangle$ directions with a length/width ratio exceeding five. Furthermore, for a substantial fraction of the surface the STM images do not show molecularly resolved features.

Besides different domain shapes, there is another structural feature which—also including the odd-numbered BP n SAMs—is only observed for BP4 prepared at elevated temperatures. A network of two different types of dark lines often connecting vacancy islands is observed. One line type consists of poorly ordered structures (e.g., Figure 6d, arrow A) separating adjacent well-ordered domains. In contrast, the other type of line marked by arrow B in Figure 6d exhibits a highly crystalline structure. This is analyzed in more detail in Figure 8. Zooming into the areas labeled A and B in Figure 8a, two different cases are identified. These are depicted in Figure 8b,c together with the corresponding height profiles which show that inside the stripes the molecules appear lower than in the surrounding area by about 0.5 \AA . The molecular packing inside the stripes is excellent; i.e., no defects due to missing molecules are seen. Comparing the contrast variations on both sides of the stripe in Figure 8b reveals a shift along the $\langle 211 \rangle$ direction, indicative of a translational domain boundary. An illustration is provided in Figure 8d. In contrast, no shift can be identified in Figure 8c, suggesting at first glance that in this case the dark line does not correspond to a translational domain boundary. Although the origin giving rise to the formation of the dark feature cannot be unambiguously identified at this point, we would like to discuss two possible explanations. The first one assumes a packing fault in the SAM. Looking at the illustration (Figure 8e), a translational domain boundary is nevertheless possible with, however, a shift within the error of our STM data. Such a small shift would mean a change in adsorption sites, e.g., from fcc to hcp. However, as a consequence, a change in electronic coupling between the substrate and the molecule is expected, and thus, a change in STM contrast should result. This is not observed and would, therefore, imply that the tunneling current is not significantly affected by such a change in adsorption site. The second model assumes a stacking fault in the substrate. This would allow for identical adsorption sites on both sides of the dark stripe and would be consistent with the absence of any changes in the structure of the SAM and the STM contrast. Since the substrate is an evaporated polycrystalline gold film, a stacking fault is conceivable. Support for this interpretation comes from etching experiments which revealed stacking faults by showing adjacent triangular etch pits which are rotated by 60° with respect to each other.⁶¹

IV. Discussion

Briefly summarizing, the main results from the above studies of BP n SAMs are the following:

First, only two basic structures are observed throughout the homologue series which are alternately adopted for $n = \text{even}$ and $n = \text{odd}$. The corresponding unit cells are pronouncedly different with two and eight molecules per unit cell for $n = \text{odd}$ and $n = \text{even}$, respectively. The intermolecular distances exhibit an odd–even alternation resulting in a packing density for $n = \text{odd}$, which is 25% denser than for $n = \text{even}$.

Second, within each category one of the molecules is somewhat different from the others. For $n = \text{odd}$ this is BP1, which exhibits a temperature-dependent formation of protruding islands. For $n = \text{even}$ this is BP6 with its strong anisotropy of the domain shape.

Before discussing the present results on BP n SAMs in more detail, it is important to briefly refer to the case of alkanethiols.³ There, for all chain lengths studied so far a $c(2\sqrt{3} \times \sqrt{3})$ (frequently referred to as $c(4 \times 2)$ structure) is observed which is basically derived from the $(\sqrt{3} \times \sqrt{3})R30^\circ$ lattice formed by the S headgroups on the substrate Au (111) surface. In this case four molecules are contained within a unit cell, and no variation of unit cell size or film structure is observed when increasing the number of methylene units. In particular, there is no odd–even effect with respect to the packing density.⁶² Only the orientation of the terminal methyl group alternates with the number of methylene units. The chains are tilted relative to the surface normal, which can be rationalized by the fact that the distance between alkane chains in the bulk amounts to about 4.6 Å, significantly less than the value of 4.99 Å between the S atoms in the $(\sqrt{3} \times \sqrt{3})R30^\circ$ overlayer on the Au substrate. For a tilt around 30° about the same density as in bulk alkanes can be realized which, thus, allows for a maximization of intermolecular interactions. At the same time the C–S–Au bond angle can adopt an sp^3 -like geometry, which seems to be the preferred one for the sulfur in an aliphatic thiol.⁶²

The very different molecular packing of odd- and even-numbered BP n SAMs which contrasts the alkanethiols SAMs is qualitatively described by a simple model based on the interplay of several factors which are crucial for the energetics of the SAMs. Since its essentials have been discussed in some detail elsewhere,^{19,47,50} only a brief summary is given here. The key point is a significant directional force due to a preferred bond angle ϕ (see Figure 1), which, for thiols on gold, can be phenomenologically described by an sp^3 -type hybridization of the sulfur. With a rather narrow shape of the Au–S–C bending potential, it is energetically costly for ϕ to deviate significantly from the optimum value. Together with intermolecular interactions, involving both biphenyl moieties and the spacers, and the thiol coverage, i.e., the number of S–Au bonds, the bending potential enters into the energy balance to a significant extent. The crucial point is that the molecular structure determines whether the bending potential enters the energy balance in a cooperative or competitive way compared to the other contributions. The driving forces to maximize the intermolecular interactions and to increase the coverage run parallel, and thus, both goals can be achieved by minimization of intermolecular distances. For a flat bending potential this would be independent from the length of the spacer; i.e., the intermolecular interactions should only increase with increasing n analogously to alkanethiols³ but should lack an odd–even alternation. A narrow bending potential, however, lifts the independence from n . A favorable value of ϕ with, at the same time, an optimized coverage and molecular packing can only be realized for $n = \text{odd}$, whereas there is a conflict for $n = \text{even}$ resulting in a structure that is a balance of these partially opposing contributions. A rough estimation of how much energy is involved, that is, how much

ϕ deviates for $n = \text{even}$ from its preferred value for $n = \text{odd}$ can be given by looking at the odd–even difference in coverage which is about 25%. Considering that the S–Au bond¹ is 185 kJ/mol, this amounts to an odd–even difference in the energy of the bending potential of up to 46 kJ/mol.⁶³ We note that this is a rather simplified picture meant to highlight the importance of the factors governing a SAM structure for a proper design of a molecular structure. It neglects other crucial contributions such as odd–even changes in the interaction energies between the molecules due to variations in packing density and the substrate corrugation, i.e., the exact adsorption sites.

Addressing the issue of adsorption sites, it is interesting to analyze how the reduced packing observed for the even-numbered BP n SAMs, i.e., the large mismatch between the lattices of the gold substrate and the monolayer, influences the molecule–molecule separation. In the STM data the distances between the protrusions assigned to the individual molecules are evenly spaced. Since, as mentioned above, we have reason to believe that the terminating methylene unit is imaged in the STM data, this could be explained by two models:

The most simple way to adsorb eight molecules in a unit cell which, in principle, could accommodate 10 molecules would be to adsorb eight molecules on the adsorption sites corresponding to a $(2\sqrt{3} \times \sqrt{3})R30^\circ$ structure and to leave two adsorption sites unoccupied. To explain the evenly spaced terminating methyl groups observed in the STM micrograph, the tilt angle of the molecules would have to vary significantly within the unit cell in order to allow the terminating CH_3 group to fill the available space in a regular fashion. Although we are presently unable to exclude this possibility, we prefer a different model which assumes that the sulfur atoms do adopt different adsorption sites. This is energetically costly as theoretical calculations^{64,65} suggest which find a difference in binding energy between bridge, hollow, and on-top adsorption sites. With regard to the present case of even-numbered BP n SAMs, we speculate that the intermolecular interactions in combination with the directional force of the C–S–Au bending potential are so strong that the small difference in binding energy for sulfur atoms placed in different adsorption sites can be overcome, so that there are up to eight different adsorption sites for the thiolate S atoms in a unit cell. We note here that the structural models proposed in Figure 9 are not fully consistent with the interpretation of high-resolution X-ray photoelectron spectroscopy (HRXPS) data⁴⁷ of BP n ($n = 1\text{--}4$). While also in this work evidence is presented that there are different S adsorption sites for even- and odd-numbered BP n 's, it has been proposed that the half-width of the XPS S_{2p} line for the even-numbered BP n 's being slightly smaller than for the odd-numbered case results from more similar S adsorption sites in the even-numbered case. To resolve this slight discrepancy and in order to allow for a comparison at this level of detail, it will be necessary to carry out high-resolution XPS measurements for samples that are prepared using the same optimized preparation conditions (in particular, elevated temperatures of the organothiol solution) employed in the present study.

As seen from the previous spectroscopic studies¹⁹ and the present STM data, the odd–even variation in packing density and orientation of the biphenyl moieties persists over a whole range of n values. This is somewhat surprising considering the fact that the BP n molecules should have an increasing number of degrees of freedom with increasing spacer chain and, therefore, should progressively be able to compensate a mismatch between the minimum value of the bending potential and maximum interaction between the BP moieties with

increasing n . Moreover, within the experimental accuracy all even-numbered SAMs adopt the same unit cell, i.e., the rather large intermolecular distance (6.25 Å compared to the 5 Å of a $\sqrt{3}$ -based lattice) is maintained despite an increase in the length of the spacer which should increase the contribution from intermolecular interactions of the methylenes as is the case for alkanethiols.³ That the interactions of the alkane chains become important and even dominant is seen by comparing phenylmethanethiol²⁵ and phenylethanethiol²⁵ ($\text{C}_6\text{H}_5(\text{CH}_2)_n\text{SH}$, $n = 1, 2$) with longer chain homologues ($n = 12-15$).⁶⁶ Whereas the packing is significantly different between $n = 1$ and $n = 2$, there is no odd–even effect in the packing density when the value of n is in the range 12–15. Only the orientation of the terminating phenyl groups was found to vary. Since intermediate values of n have not been investigated, it is not clear at present where the transition region exactly lies and how wide it is for phenylalkanethiols.

Such a transition from structures that are determined by interactions of the aromatic moieties and the C–S–Au bending potential to another structure that is determined by the alkane–alkane packing is also to be expected for the BP n SAMs, and in fact, we believe that BP6 marks the onset of this transition. In contrast to all other BP n SAMs where the overall quality of the layer, that is, the domain size, improves with increasing preparation temperature, BP6 behaves differently. For BP6 (Figure 7d) the structural quality is surprisingly poor compared to all other structures.

Well-ordered areas coexist with areas where weak or no molecularly resolved features are seen. Since the ordered domains are rather small, no contrast variation indicative of a lattice mismatch can be identified. Phenomenologically, it is clear that a rectangular adsorbate structure whose azimuthal alignment is determined by a substrate with 3-fold symmetry cannot be densely packed. However, at the molecular level the details of the strongly anisotropic domain shape are not fully clear, and therefore, only a tentative, incomplete picture can be presented here. It is surprising that the domain shape is rectangular and not oblique since a domain boundary along $\langle 211 \rangle$ represents a rather open structure whereas an oblique geometry parallel to the dotted lines in Figure 9b is more closely packed on all sides. The experimental observation that growth along $\langle 110 \rangle$ is preferred compared to $\langle 211 \rangle$ can be rationalized by assuming azimuthally anisotropic intermolecular interactions. Compared to the $\sqrt{3} \times \sqrt{3}$ -based unit cell of normal alkanethiols, the unit cells of even-numbered BP n SAMs are substantially stretched along the $\langle 211 \rangle$ direction, which increases the intermolecular distance along this direction from 5 to 6.25 Å. As a result, the intermolecular interactions are stronger in the $\langle 110 \rangle$ direction, along which the domains then grow preferentially. Even though this structural anisotropy is present in all even-numbered BP n SAMs, any possible anisotropy in intermolecular interactions seems insufficient to express itself on a larger length scale for $n < 6$. Since the length of the spacer chain is the only difference within the homologue series of even-numbered BP n SAMs, this implies that for $n = 6$ the length of the alkane spacer has become long enough to play an appreciable role in the energetics of the system. While it appears that the azimuthal anisotropy of the intermolecular interactions of the aromatic units is too small for a strongly anisotropic domain growth, the alkane spacers seem to introduce such an anisotropy. It cannot be said at present whether this is due to direct interaction between the chains and/or whether increased conformational degrees of freedom due to the longer alkane spacer yields a subtle rearrangement of the BP units which lifts the isotropy.

Nevertheless, the case of BP6 demonstrates that the energetics and structure of BP n SAMs is determined by the balance of contributions from the S–Au interface (coverage, C–S–Au bending potential), the BP units, and the spacer chain. The latter requires a minimum length to enter into the balance to a significant extent. This implies that BP6 is at the beginning of a transition region where the SAM changes from a structure that is determined by the biphenyl moieties and the directional force from the S–Au interface to a structure determined by the interactions of the alkane chains. Future experiments with $n > 6$ have to substantiate such a structural evolution.

While comparison of the BP6 SAMs prepared at room (Figure 7c) and elevated temperature (Figure 7d) reveals no significant differences in the unit cells, the domains in films prepared at room temperature do not show any sign of anisotropy. This indicates that a SAM structure can well be determined by kinetic rather than thermodynamic factors and can easily become trapped in a local minimum of the free enthalpy.

We close the discussion with a comparison of the BP1 SAMs prepared at room temperature (Figure 2a,c) and at 343 K (Figure 2f,g) where only in the latter case formation of small protrusions was observed. Although the small size of these features makes its analysis difficult, the height of these features of about 2.5 Å could be explained by the formation of the small Au islands. In fact, the formation of Au islands which contrast the vacancy island formation observed for SAMs of aliphatic thiols was already reported for other aromatic thiol SAMs on Au(111). According to a model proposed very recently by Yang and Liu,²⁵ formation of both adatom islands and vacancy islands originates from lifting of the original $(23 \times \sqrt{3})$ reconstruction of the Au(111) surface after thiol adsorption. Formation of adatom islands was suggested to depend on the activation energy for diffusion of gold adatoms. The difference in this activation energy for aliphatic and aromatic thiols SAMs was ascribed to differences in the Au–S bond energy, which depends on whether the sulfur is attached to an aliphatic or aromatic unit, respectively. For aromatic thiols a lower activation energy was concluded. The observations of adatom islands for BP1 SAMs investigated here cannot be explained by this model. First, in contrast to all other systems where adatom islands have been observed,^{12,21,22,25,67} the sulfur is not directly attached to the aromatic system and, thus, should be only weakly affected by the aromatic unit. Second and more importantly, the adatom island formation only appears at elevated temperatures. This is in conflict with the suggested model since an increase in temperature should facilitate diffusion, and thus, islands should disappear rather than appear. At this point we would like to add that adatom island formation just by lifting of the gold reconstruction is also not able to explain data obtained by Jin et al.¹² In their experiments up to 50% of the surface was covered by islands, far too much to be solely attributed to the relaxation of the $(23 \times \sqrt{3})$ reconstruction which releases only 4.4% of a monolayer of gold atoms. It appears that factors in addition to diffusion play a role. Further experiments have to show to what extent other kinetic factors and/or thiol induced stress control the formation of adatom islands.

V. Conclusion

As evidenced by the odd–even variation in the structures of BP n SAMs, the film structure exhibits a pronounced dependence on the molecular structure. In the present case it is the odd–even variation and overall length of the spacer chain which controls the balance between factors governing the energetics of thiol layers. The evolution of anisotropy in the even-numbered

BPn SAMs from $n = 2$ to 6 gives a clear demonstration how sensitively the film structure depends on the molecular structure.

The influence of preparation temperature strongly varies with the system. Both island formation for BP1 and appearance of disordered regions for BP6 at elevated temperatures clearly show limitations with respect to the achievable structural quality since limitations are imposed on the temperature treatment as a way to increase domain size and anneal vacancy islands.

An important parameter that has not been fully appreciated and explored so far is the C–S substrate bending potential. Design concepts have focused on energy minimization and, thus, the cooperative influence of the bending potential and intermolecular interactions. This is reflected by using molecules with one methyl group between the aromatic unit and the thiol group to match a favorable C–S substrate bond angle with an optimum packing of the molecules.^{10,22,44} The even-numbered SAMs investigated here indicate that a design based on competitive factors can introduce an additional route to tailor the structure of SAMs.

Acknowledgment. This work was supported by The Leverhulme Trust, German Science Foundation, Scottish Higher Education Funding Council (SHEFC), and EPSRC.

References and Notes

- Ulman, A. *Chem. Rev.* **1996**, *96*, 1533–1554.
- Schwartz, D. K. *Annu. Rev. Phys. Chem.* **2001**, *52*, 107–137.
- Schreiber, F. *Prog. Surf. Sci.* **2000**, *65*, 151–256.
- Wong, S. S.; Porter, M. D. *J. Electroanal. Chem.* **2000**, *485*, 135–143.
- Becka, A. M.; Miller, C. J. *J. Phys. Chem.* **1993**, *97*, 6233–6239.
- Chidsey, C. E. D.; Bertozzi, C. R.; Putvinski, T. M.; Mujcs, A. M. *J. Am. Chem. Soc.* **1990**, *112*, 4301–4306.
- Byloos, M.; Al-Mazna, H.; Morin, M. *J. Phys. Chem. B* **1999**, *103*, 6554–6561.
- Tour, J. M.; Jones, L.; Pearson, D. L.; Lamba, J. J. S.; Burgin, T. P.; Whitesides, G. M.; Allara, D. L.; Parikh, A. N.; Atre, S. V. *J. Am. Chem. Soc.* **1995**, *117*, 9529–9534.
- Bumm, L. A.; Arnold, J. J.; Cygan, M. T.; Dunbar, T. D.; Burgin, T. P.; Jones, L.; Allara, D. L.; Tour, J. M.; Weiss, P. S. *Science* **1996**, *271*, 1705–1707.
- Tao, Y. T.; Wu, C. C.; Eu, J. Y.; Lin, W. L. *Langmuir* **1997**, *13*, 4018–4023.
- Zehner, R. W.; Sita, L. R. *Langmuir* **1997**, *13*, 2973–2979.
- Jin, Q.; Rodriguez, J. A.; Li, C. Z.; Darici, Y.; Tao, N. J. *Surf. Sci.* **1999**, *425*, 101–111.
- Ishida, T.; Mizutani, W.; Aya, Y.; Ogiso, H.; Sasaki, S.; Tokumoto, H. *J. Phys. Chem. B* **2002**, *106*, 5886–5892.
- Wold, D. J.; Haag, R.; Rampi, M. A.; Frisbie, C. D. *J. Phys. Chem. B* **2002**, *106*, 2813–2816.
- Ishida, T.; Mizutani, W.; Akiba, U.; Umemura, K.; Inoue, A.; Choi, N.; Fujihira, M.; Tokumoto, H. *J. Phys. Chem. B* **1999**, *103*, 1686–1690.
- Rampi, M. A.; Whitesides, G. M. *Chem. Phys.* **2002**, *281*, 373–391.
- Cui, X. D.; Primak, A.; Zarate, X.; Tomfohr, J.; Sankey, O. F.; Moore, A. L.; Moore, T. A.; Gust, D.; Harris, G.; Lindsay, S. M. *Science* **2001**, *294*, 571–574.
- Leung, T. Y. B.; Schwartz, P.; Scoles, G.; Schreiber, F.; Ulman, A. *Surf. Sci.* **2000**, *458*, 34–52.
- Rong, H. T.; Frey, S.; Yang, Y. J.; Zharnikov, M.; Buck, M.; Wöhl, C.; Helmchen, G. *Langmuir* **2001**, *17*, 1582–1593.
- Ulman, A. *Acc. Chem. Res.* **2001**, *34*, 855–863.
- Azzam, W.; Fuxen, C.; Birkner, A.; Rong, H. T.; Buck, M.; Wöhl, C. *Langmuir* **2003**, *19*, 4958–4968.
- Fuxen, C.; Azzam, W.; Arnold, R.; Witte, G.; Terfort, A.; Wöhl, C. *Langmuir* **2001**, *17*, 3689–3695.
- Garg, N.; Carrasquillo-Molina, E.; Lee, T. R. *Langmuir* **2002**, *18*, 2717–2726.
- Baunach, T.; Kolb, D. M. *Anal. Bioanal. Chem.* **2002**, *373*, 743–748.
- Yang, G. H.; Liu, G. Y. *J. Phys. Chem. B* **2003**, *107*, 8746–8759.
- Frey, S.; Stadler, V.; Heister, K.; Eck, W.; Zharnikov, M.; Grunze, M.; Zeysing, B.; Terfort, A. *Langmuir* **2001**, *17*, 2408–2415.
- Kang, J. F.; Ulman, A.; Liao, S.; Jordan, R.; Yang, G. H.; Liu, G. Y. *Langmuir* **2001**, *17*, 95–106.
- Geyer, W.; Stadler, V.; Eck, W.; Zharnikov, M.; Götzhäuser, A.; Grunze, M. *Appl. Phys. Lett.* **1999**, *75*, 2401–2403.
- Sikes, H. D.; Smalley, J. F.; Dudek, S. P.; Cook, A. R.; Newton, M. D.; Chidsey, C. E. D.; Feldberg, S. W. *Science* **2001**, *291*, 1519–1523.
- Creager, S.; Yu, C. J.; Bamdad, C.; O'Connor, S.; MacLean, T.; Lam, E.; Chong, Y.; Olsen, G. T.; Luo, J. Y.; Gozin, M.; Kayyem, J. F. *J. Am. Chem. Soc.* **1999**, *121*, 1059–1064.
- Felgenhauer, T.; Rong, H. T.; Buck, M. *J. Electroanal. Chem.* **2003**, *550*, 309–319.
- Fan, F. R. F.; Yang, J. P.; Cai, L. T.; Price, D. W.; Dirk, S. M.; Kosynkin, D. V.; Yao, Y. X.; Rawlett, A. M.; Tour, J. M.; Bard, A. J. *J. Am. Chem. Soc.* **2002**, *124*, 5550–5560.
- Adams, D. M.; Brus, L.; Chidsey, C. E. D.; Creager, S.; Creutz, C.; Kagan, C. R.; Kamat, P. V.; Lieberman, M.; Lindsay, S.; Marcus, R. A.; Metzger, R. M.; Michel-Beyerle, M. E.; Miller, J. R.; Newton, M. D.; Rolison, D. R.; Sankey, O.; Schanze, K. S.; Yardley, J.; Zhu, X. Y. *J. Phys. Chem. B* **2003**, *107*, 6668–6697.
- Aslam, M.; Chaki, N. K.; Sharma, J.; Vijayamohan, K. *Curr. Appl. Phys.* **2003**, *3*, 115–127.
- Zehner, R. W.; Parsons, B. F.; Hsung, R. P.; Sita, L. R. *Langmuir* **1999**, *15*, 1121–1127.
- Felgenhauer, T.; Yan, C.; Geyer, W.; Rong, H. T.; Götzhäuser, A.; Buck, M. *Appl. Phys. Lett.* **2001**, *79*, 3323–3325.
- Di Ventura, M.; Pantelides, S. T.; Lang, N. D. *Phys. Rev. Lett.* **2000**, *84*, 979–982.
- Emberly, E. G.; Kirczenow, G. *Phys. Rev. B* **2001**, *64*, 235412.
- Kornilovitch, P. E.; Bratkovsky, A. M. *Phys. Rev. B* **2001**, *64*, 195413.
- Bratkovsky, A. M.; Kornilovitch, P. E. *Phys. Rev. B* **2003**, *67*, 115307.
- Nitzan, A. *Annu. Rev. Phys. Chem.* **2001**, *52*, 681–750.
- Naaman, R.; Haran, A.; Nitzan, A.; Evans, D.; Galperin, M. *J. Phys. Chem. B* **1998**, *102*, 3658–3668.
- Cui, X. D.; Primak, A.; Zarate, X.; Tomfohr, J.; Sankey, O. F.; Moore, A. L.; Moore, T. A.; Gust, D.; Nagahara, L. A.; Lindsay, S. M. *J. Phys. Chem. B* **2002**, *106*, 8609–8614.
- Ishida, T.; Mizutani, W.; Choi, N.; Akiba, U.; Fujihira, M.; Tokumoto, H. *J. Phys. Chem. B* **2000**, *104*, 11680–11688.
- Haran, A.; Kadyshkevitch, A.; Cohen, H.; Naaman, R.; Evans, D.; Seideman, T.; Nitzan, A. *Chem. Phys. Lett.* **1997**, *268*, 475–480.
- Miller, A. D.; Gaffney, K. J.; Liu, S. H.; Szymanski, P.; Garrett-Roe, S.; Wong, C. M.; Harris, C. B. *J. Phys. Chem. A* **2002**, *106*, 7636–7638.
- Heister, K.; Rong, H. T.; Buck, M.; Zharnikov, M.; Grunze, M.; Johansson, L. S. O. *J. Phys. Chem. B* **2001**, *105*, 6888–6894.
- Long, Y. T.; Rong, H. T.; Buck, M.; Grunze, M. *J. Electroanal. Chem.* **2002**, *524*, 62–67.
- Frey, S.; Rong, H. T.; Heister, K.; Yang, Y. J.; Buck, M.; Zharnikov, M. *Langmuir* **2002**, *18*, 3142–3150.
- Azzam, W.; Cyganik, P.; Witte, G.; Buck, M.; Wöhl, C. *Langmuir* **2003**, *19*, 8262–8270.
- Zharnikov, M.; Frey, S.; Rong, H.; Yang, Y. J.; Heister, K.; Buck, M.; Grunze, M. *Phys. Chem. Chem. Phys.* **2000**, *2*, 3359–3362.
- Noh, J.; Hara, M. *Langmuir* **2001**, *17*, 7280–7285.
- Edinger, K.; Götzhäuser, A.; Demota, K.; Wöhl, C.; Grunze, M. *Langmuir* **1993**, *9*, 4–8.
- Poirier, G. E. *Langmuir* **1997**, *13*, 2019–2026.
- McDermott, C. A.; McDermott, M. T.; Green, J. B.; Porter, M. D. *J. Phys. Chem.* **1995**, *99*, 13257–13267.
- Sondag-Huethorst, J. A. M.; Schonenberger, C.; Fokink, L. G. J. *J. Phys. Chem.* **1994**, *98*, 6826–6834.
- Poirier, G. E.; Tarlov, M. J. *J. Phys. Chem.* **1995**, *99*, 10966–10970.
- Cavalleri, O.; Hirstein, A.; Kern, K. *Surf. Sci.* **1995**, *340*, L960–L964.
- Bumm, L. A.; Arnold, J. J.; Charles, L. F.; Dunbar, T. D.; Allara, D. L.; Weiss, P. S. *J. Am. Chem. Soc.* **1999**, *121*, 8017–8021.
- Cyganik, P.; Buck, M.; Wöhl, C. Manuscript in preparation.
- Cyganik, P.; Felgenhauer, T.; Rong, H.-T.; Buck, M.; Postawa, Z. *Electron Technol.* **2000**, *33*, 337–343.
- Laibinis, P. E.; Whitesides, G. M.; Allara, D. L.; Tao, Y. T.; Parikh, A. N.; Nuzzo, R. G. *J. Am. Chem. Soc.* **1991**, *113*, 7152–7167.
- The value of about 15–20 kJ/mol given in ref 19 is somewhat lower since the odd–even difference was derived from spectroscopic data which detected a difference of less than 20% possibly due to the averaging of well and less well ordered areas/domain boundaries.
- Gottschalk, J.; Hammer, B. *J. Chem. Phys.* **2002**, *116*, 784–790.
- Hayashi, T.; Morikawa, Y.; Nozoye, H. *J. Chem. Phys.* **2001**, *114*, 7615–7621.
- Lee, S.; Puck, A.; Graupe, M.; Colorado, R.; Shon, Y. S.; Lee, T. R.; Perry, S. S. *Langmuir* **2001**, *17*, 7364–7370.
- Dhirani, A. A.; Zehner, R. W.; Hsung, R. P.; Guyot-Sionnest, P.; Sita, L. R. *J. Am. Chem. Soc.* **1996**, *118*, 3319–3320.